Molecular Medicine

Galectin-3 Ablation Enhances Liver Steatosis, but Attenuates Inflammation and IL-33-Dependent Fibrosis in Obesogenic Mouse Model of Nonalcoholic Steatohepatitis

Ilija Jeftic,[1,2] Nemanja Jovicic,[1,3] Jelena Pantic,[1] Nebojsa Arsenijevic,[1] Miodrag L Lukic,[1] and Nada Pejnovic[1,2]

[1]Center for Molecular Medicine and Stem Cell Research, [2]Institute of Pathophysiology, and [3]Institute of Histology, Faculty of Medical Sciences, University of Kragujevac, Kragujevac, Serbia

The importance of Galectin-3 (Gal-3) in obesity-associated liver pathology is incompletely defined. To dissect the role of Gal-3 in fibrotic nonalcoholic steatohepatitis (NASH), Gal-3-deficient (LGALS3$^{-/-}$) and wild-type (LGALS3$^{+/+}$) C57Bl/6 mice were placed on an obesogenic high fat diet (HFD, 60% kcal fat) or standard chow diet for 12 and 24 wks. Compared to WT mice, HFD-fed LGALS3$^{-/-}$ mice developed, in addition to increased visceral adiposity and diabetes, marked liver steatosis, which was accompanied with higher expression of hepatic *PPAR-γ*, *Cd36*, *Abca-1* and *FAS*. However, as opposed to LGALS3$^{-/-}$ mice, hepatocellular damage, inflammation and fibrosis were more extensive in WT mice which had an elevated number of mature myeloid dendritic cells, proinflammatory CD11b^{+}Ly6C^{hi} monocytes/macrophages in liver, peripheral blood and bone marrow, and increased hepatic *CCL2, F4/80, CD11c, TLR4, CD14, NLRP3* inflammasome, *IL-1β* and *NADPH*-oxidase enzymes mRNA expression. Thus, obesity-driven greater steatosis was uncoupled with attenuated fibrotic NASH in Gal-3-deficient mice. HFD-fed WT mice had a higher number of hepatocytes that strongly expressed IL-33 and hepatic CD11b^{+}IL-13^{+} cells, increased levels of IL-33 and IL-13 and upregulated *IL-33, ST2* and *IL-13* mRNA in liver compared with LGALS3$^{-/-}$ mice. IL-33 failed to induce ST2 upregulation and IL-13 production by LGALS3$^{-/-}$ peritoneal macrophages *in vitro*. Administration of IL-33 *in vivo* enhanced liver fibrosis in HFD-fed mice in both genotypes, albeit to a significantly lower extent in LGALS3$^{-/-}$ mice, which was associated with less numerous hepatic IL-13-expressing CD11b^{+} cells. The present study provides evidence of a novel role for Gal-3 in regulating IL-33-dependent liver fibrosis.

Online address: http://www.molmed.org
doi: 10.2119/molmed.2014.00178

INTRODUCTION

Nonalcoholic fatty liver disease (NAFLD), which encompasses simple steatosis, nonalcoholic steatohepatitis (NASH), cirrhosis and possibly liver carcinoma, is strongly associated with obesity and metabolic syndrome and patients with type 2 diabetes are predisposed to develop a more severe form of fibrotic NASH (1,2). During obesity, immune cells infiltrated in visceral adipose tissue mediate chronic low-grade inflammation that plays a key role in the pathogenesis of NAFLD (1,3). In the progression from steatosis to NASH, fat deposition renders hepatocytes susceptible to inflammatory, lipid and oxidative stress mediators through as yet incompletely defined molecular mechanisms, resulting in liver inflammation and damage (3). In NASH, through secreted chemokines and cytokines, intrahepatic innate and adaptive immune cells sustain chronic inflammation and induce transdifferentiation of hepatic stellate cells (HSCs) into myofibroblasts, key cells in liver fibrosis (4).

Galectin-3 (Gal-3), the unique "chimera-type" β-galactoside-binding lectin, exerts both pro- and antiinflammatory roles, depending on disease condition. There is plethora of evidence of its proinflammatory role in immune-mediated inflammation (5–7) and organ-specific autoimmunity (8). However, Gal-3 attenuates macrophage sensitivity to endotoxin (9) and has a protective role in the setting of high-fat diet-induced obesity, adipose tissue inflammation, diabetes and atherosclerosis, partly by its ability to scavenge advanced glycation end products (AGE) and downregulate receptor for AGE (RAGE), thus preventing the consequent RAGE-dependent inflammation (10–12). Obese Gal-3-deficient mice had enhanced activation of NLRP3 inflammasome and NFκB in

*IJ and NJ contributed equally to this study.

Address correspondence to *Miodrag L Lukic, Center for Molecular Medicine and Stem Cell Research, Faculty of Medical Sciences, University of Kragujevac, Svetozara Markovica 69, 34000 Kragujevac, Serbia. Phone: +381-34-306-800; Fax: +381-34-306-800112; E-mail: miodrag.lukic@medf.kg.ac.rs.*

Submitted September 10, 2014; Accepted for publication May 21, 2015; Published Online (www.molmed.org) May 22, 2015.

adipose tissue and islets where dendritic cells (DCs) and macrophages play important roles (11).

The data on the effect of Gal-3 ablation in liver steatosis/inflammation are controversial. Nomoto *et al*. (13) showed that Gal-3-deficient mice spontaneously developed steatosis at six months of age and that a lack of Gal-3 led to greater steatosis and liver injury in the model of CDAA diet-induced NASH (14). On the other hand, in a study by Iacobini *et al*. (15) Gal-3 null mice fed an atherogenic diet were resistant to the development of steatosis and NASH. In the liver, Gal-3 is highly expressed in Kupffer cells and its expression is increased during hepatocellular damage (16). The essential step in hepatic inflammation and fibrogenesis is CCL2-mediated monocyte recruitment (17,18). Resident and recruited liver macrophages may be polarized toward classically activated macrophages (M1), which promote survival of hepatic myofibroblasts by secreted TNF-α and IL-1β, and, alternatively, macrophages that express the Th2-type cytokines (M2), including IL-13, which directly stimulates collagen synthesis in myofibroblasts (19–21). Macrophage-derived Gal-3 has been shown to promote myofibroblast activation in liver fibrosis (22,23). The disruption of the Gal-3 gene was reported to block TGF-β mediated myofibroblast activation and procollagen expression and markedly attenuated CCl_4-induced liver fibrosis in mice (22). Interleukin-33 (IL-33), a damage-associated molecular pattern (DAMP) molecule, could induce IL-13 production by macrophages to promote type 2 immunity (24). IL-33 has a profibrogenic role through ST2-dependent (IL-33 receptor–dependent) production of IL-13 by innate lymphoid cells (ILCs) that activates hepatic stellate cells (HSCs) and promotes liver fibrosis (25,26). Recent data suggest that IL-13, rather than TGF-β, predominantly activates HSCs in liver fibrosis (27). The role of Gal-3 in the regulation of profibrogenic IL-33/ST2/IL-13 pathways has not been studied.

To delineate the role of Gal-3 in obesity-associated fibrotic NASH, we investigated the effect of Gal-3 deficiency in mice using the model of high-fat diet-induced obesity and performed metabolic, gene expression, histological and immunophenotypical analyses. IL-33 administered *in vivo* enhanced liver fibrosis in WT and LGALS3$^{-/-}$ mice, and to a significantly lesser extent in Gal-3-deficient mice. The obtained results demonstrate that, in the absence of Gal-3, obesity-driven enhanced steatosis was uncoupled from attenuated hepatic fibroinflammatory response, which was associated with less numerous hepatic proinflammatory DCs and macrophages and attenuated profibrogenic IL-33/IL-13 pathway.

MATERIALS AND METHODS

Mice, Dietary Model and IL-33 Administration

Eight-week-old male Gal-3-deficient (LGALS3$^{-/-}$) mice on the C57BL/6 background and their littermate controls, wild-type (WT) C57BL/6 mice, obtained from the University of California Davis (Davis, CA; by courtesy of DK Hsu and FT Liu) were fed either standard chow diet (CHOW; 10% kcal fat content) or high-fat diet (HFD; 60% kcal fat content) obtained from Mucedola (Milano, Italy) *ad libitum* for 12 and 24 wks. In some experiments, after 10 wks on HFD, WT and LGALS3$^{-/-}$ mice were injected intraperitoneally five times every other day at 0.5 μg per injection, with murine recombinant IL-33 (R&D Systems, Minneapolis, MN, USA) or PBS. Mice were euthanized and bone marrow, blood samples, liver, colon and visceral adipose tissue from epididymal and perirenal pads were collected for analyses. All animal procedures were approved by the Ethical Committee of the Faculty of Medical Sciences, University of Kragujevac.

Metabolic Parameters

Body weights and fasting blood glucose levels were measured once every 4 wks. Mice were fasted for 4 h and glucose levels (mmol/L) were determined using the Accu-Chek Performa Glucometer (Roche Diagnostics, Mannheim, Germany). Serum concentrations of lipids, AST and ALT activity were measured using the Olympus AU600 Chemistry Immuno Analyzer (Olympus, Tokyo, Japan) and fasting insulin using Insulin ELISA kit (Alpco, Salem, NH, USA). HOMA-IR was calculated as described previously (28).

Histopathological Analyses

Paraffin-embedded liver and colon sections (5 μm) were stained with H&E for the assessment of the degree of inflammation (29,30). Oil red O staining was used to assess hepatic lipid deposition. Picrosirius red (Direct Red 80, Sigma-Aldrich, St. Louis, MO, USA) and Masson trichrome (Sigma-Aldrich, Trichrome Stain Masson Kit) staining were used to assess hepatic collagen deposition. NAS activity score was determined as described (29). Quantification of steatosis and fibrosis in mouse liver sections stained with oil red O (100×) and picrosirius red (10×) was performed using ImageJ software (National Institutes of Health, Bethesda, MD, USA; http://rsb.info.nih.gov/ij/), on 10 fields/section, as described previously (31,32). Scoring and histological analysis were performed in blinded fashion by two independent observers.

Liver Immunohistochemical Analyses

For immunohistochemical staining, deparaffinized liver tissue sections were incubated with primary mouse anti-CD68 (ab49777, Abcam, Cambridge, UK), primary mouse anti-α-SMA (ab7817, Abcam), primary rabbit anti-Gal-3 antibody (ab53082, Abcam) and primary rabbit anti-IL-33 antibody (M-266, Santa Cruz Biotechnology, Santa Cruz, CA, USA). Staining was visualized by using mouse specific HRP/DAB detection IHC Kit (ab64259, Abcam) for CD68 and α-SMA and rabbit specific HRP/AEC detection IHC Kit (ab94361, Abcam) for Gal-3 and

IL-33. Sections were photomicrographed with a digital camera mounted on light microscope (Olympus BX51, Japan), digitized and analyzed. Analysis was performed on 10 fields/section (×40). Results are presented as a mean count of positive stained cells per field.

Isolation of Liver Mononuclear, Peripheral Blood and Bone Marrow Cells

The isolation of liver mononuclear cells was performed as described previously (33). Anticoagulant-treated blood was used for analyses of peripheral blood cells (PBCs). Bone marrow cells (BMCs) were removed from both femurs of each mouse as described (34). After red blood cell lysis, PBCs and BMCs were resuspended in FACS staining buffer for flow cytometric analysis.

IL-33 Stimulation of Macrophages *In Vitro*

Peritoneal cells were collected from the peritoneal cavity of WT and LGALS3$^{-/-}$ mice under sterile conditions and allowed to adhere to glass petri dishes for 2 h at 37°C. Adherent macrophages (5×10^5 cells/24-well plate) were cultured in complete Dulbecco modified Eagle medium (Sigma-Aldrich) supplemented with 10% FCS at 37°C in a 5% CO_2 incubator and incubated with mouse recombinant IL-33 (R&D Systems) at concentrations of 20, 50 and 100 ng/mL for 48 h. After incubation, the cell supernatants were collected and cells were labeled with anti-CD11b (BD Pharmingen [BD, Franklin Lakes, NJ, USA]), anti-ST2 (R&D Systems) and anti-IL-13 (eBioscience, San Diego, CA, USA) fluorochrome-conjugated monoclonal antibodies or isotype matched controls for flow cytometry. The levels of IL-13 in cell supernatants were determined using mouse Duoset ELISA kits (R&D Systems).

Flow Cytometry

Cells were labeled with fluorochrome-conjugated monoclonal antibodies: CD3 (145-2C11), CD4 (H129.19), CD45 (30-F11), CD11b (M1/70), CD11c (N418), MHC class II (14-4-4S), CD8a (53-6.7), CD80 (16-10A1), CD86 (GL1), CCR7 (4B12), CD45R B220 (RA3-6B2), F4/80 (CI:A3-1), CD206 (MR5D3), Ly6G (1A8), Ly6C (HK1.4), ST2 (245707) or isotype matched controls (BD; eBioscience; BioLegend, San Diego, CA, USA). For intracellular staining, cells were activated with PMA (50 ng/mL)/ionomycin (500 ng/mL) (Sigma-Aldrich) with Golgy Stop (BD) for 4 h and stained with fluorochrome-labeled anti-mouse mAb specific for IL-1β (NJTEN3, eBioscience) and IL-13 (eBio13A, eBioscience). Cells were analyzed with the FACSCalibur Flow Cytometer (BD Biosciences, San Jose, CA) and FlowJo (Tree Star, Ashland, OR, USA).

Cytokine Measurements

The liver tissues were weighed and a 100 mg portion of the left lobe of the liver was homogenized in 0.5 mL PBS. Liver homogenates were centrifuged at 14,000*g* for 10 min at 4°C. Supernatants were transferred to clean microcentrifuge tubes and stored at –20°C. Cytokine levels in mouse sera and liver supernatants were determined using mouse Duoset enzyme-linked immunosorbent assay (ELISA) kits for IL-1β, IL-6, TNF-α, IFN-γ, IL-17, IL-23, IL-33, IL-13, IL-10 and TGF-β (R&D Systems) according to the manufacturer's instructions.

Limulus Amebocyte Lysate (LAL) Assay

Systemic endotoxin levels were measured using the LAL assay (Pierce LAL Chromogenic Endotoxin Quantitation Kit, Thermo Scientific [Thermo Fisher Scientific Inc., Waltham, MA, USA]) according to the manufacturer's protocol.

Quantitative RT-PCR

Total RNA from mouse liver was extracted using TRIzol reagent (Invitrogen [Thermo Fisher Scientific]) according to the manufacturer's instructions. Total RNA (2 μg) was reverse-transcribed using High Capacity cDNA Reverse Transcription Kit (Applied Biosystems [Thermo Fisher Scientific]). Real time quantitative PCR was performed using Power SYBR MasterMix (Applied Biosystems [Thermo Fisher Scientific]) and mRNA specific primers for *procollagen1A(I)*, *α-SMA*, *CD11c*, *F4/80*, *CCL2*, *NLRP3* inflammasome, *procaspase 1*, *IL-1β*, *IL-6*, *TNF-α*, *IL-33*, *ST2*, *IL-13*, *TGF-β*, *TLR-4*, *CD14*, *ChREBP*, *LXR-α*, *LXR-β*, *SREBP-1c*, *PPAR-γ*, *Abca-1*, *CD36*, *FAS*, *DAGT1*, *DAGT2*, *CPT1*, *Nox2*, $p22^{phox}$, $p47^{phox}$, $p65^{phox}$ and *β-actin* as a housekeeping gene (Invitrogen [Thermo Fisher Scientific]) (Supplementary Table 1). PCR reactions were done in a Mastercycler ep realplex (Eppendorf, Hamburg, Germany). The fold change of mRNA gene expression was calculated as described previously (35).

Statistical Analysis

Statistical analysis was performed using SPSS 13.0. Data are presented as means ± SEM (standard error of the mean). Statistical significance was determined by Student *t* test and, where appropriate, using Mann–Whitney *U* test. Statistical significance was assumed at $p < 0.05$.

All supplementary materials are available online at www.molmed.org.

RESULTS

Galectin-3 Ablation Accelerated HFD-Induced Obesity and Obesity-Related Metabolic Alterations

Body weight, weight gain and the amount of visceral adipose tissue (VAT) were significantly higher in HFD-fed LGALS3$^{-/-}$ mice compared with HFD-fed WT mice for 24 wks (Table 1). HFD feeding resulted in increased weight gain (% body weight) and visceral fat mass (% body weight) in both genotypes of mice, more pronounced in HFD-fed LGALS3$^{-/-}$ mice compared

Table 1. Metabolic parameters.[a]

	WT CHOW	WT HFD	LGALS3$^{-/-}$ CHOW	LGALS3$^{-/-}$ HFD
Body weight (g)	28.01 ± 0.5	31.07 ± 1.12[b]	29.66 ± 0.86[c]	39.51 ± 1.51[d,e]
Weight gain (g)	6.13 ± 0.33	9.54 ± 1.02[b]	7.91 ± 0.97[c]	17.7 ± 1.83[c,d]
Total VAT (g)	0.45 ± 0.02	1.21 ± 0.22[d]	0.56 ± 0.08	2.81 ± 0.33[d,e]
Liver (g)	1.39 ± 0.03	1.34 ± 0.05	1.46 ± 0.13	1.72 ± 0.13[c]
Cholesterol (mmol/L)	3.18 ± 0.17	4.76 ± 0.13[d]	3.40 ± 0.16	5.96 ± 0.22[d,e]
Triglycerides (mmol/L)	1.34 ± 0.07	1.35 ± 0.09	1.48 ± 0.11	1.74 ± 0.07[c]
Fasting blood glucose (mmol/L)	7.16 ± 0.27	7.34 ± 0.21	8.79 ± 0.31[e]	10.67 ± 0.36[d,e]
Fasting insulin (ng/mL)	0.36 ± 0.16	0.36 ± 0.12	0.39 ± 0.06	1.87 ± 0.19[b,c]
HOMA-IR	1.04 ± 0.08	1.52 ± 0.39	4.39 ± 0.89[c]	8.65 ± 1.87[b,c]
AST (IU/L)	86.2 ± 4.77	101.8 ± 4.14[b]	65.5 ± 7.51	64.5 ± 1.72[c]
ALT (IU/L)	28.5 ± 1.87	52.6 ± 6.14[b]	23.5 ± 2.25	27.25 ± 3.01[c]

[a]Eight-week-old male LGALS3$^{-/-}$ mice and WT mice were placed on HFD or standard diet for 24 wks. The results are shown as the means ± SEM (n = five to six mice/group/experiment). The results are representative of two repeated experiments.
[b]$P < 0.05$ versus CHOW-fed mice.
[c]$P < 0.05$ versus WT mice.
[d]$P < 0.01$ versus CHOW-fed mice.
[e]$P < 0.01$ versus WT mice.

with diet-matched WT mice (Supplementary Figure 1A). Total serum cholesterol and triglycerides, fasting blood glucose levels, insulinemia and HOMA-IR were significantly higher in obese LGALS3$^{-/-}$ mice compared with WT mice (Table 1). The significantly increased body weight (26.96 ± 0.36 versus 23.23 ± 0.28 g, $p = 0.011$) and fasting glycemia (9.36 ± 0.36 versus 7.20 ± 0.28 mmol/L, $p = 0.006$) were noticed in LGALS3$^{-/-}$ mice compared with WT mice, both on HFD after 4 wks. Standard diet feeding for 24 wks resulted in increased body weight, weight gain, fasting glycemia and HOMA-IR in LGALS3$^{-/-}$ mice compared with WT mice, with no difference in other metabolic parameters (Table 1). There was no difference in food intake between LGALS3$^{-/-}$ and WT mice (data not shown).

Absence of Gal-3 Resulted in Marked Steatosis, but Attenuated Liver Inflammation and Fibrosis in Mice on HFD

Firstly, we show that the protein and Gal-3 mRNA expression increased in livers of WT mice fed HFD for 24 wks compared with chow-fed controls (Figure 1A). We next examined the effects of Gal-3 deletion on hepatic steatosis, liver injury, inflammation and fibrosis in HFD-fed WT and LGALS3$^{-/-}$ mice. Oil red O and H&E stained liver sections demonstrated liver steatosis in HFD-fed animals of both genotypes, which was more pronounced in LGALS3$^{-/-}$ mice (Figures 1B, C). Despite marked liver steatosis, LGALS3$^{-/-}$ mice did not develop hepatocellular injury and liver inflammation, as indicated by the absence of hepatocyte ballooning and inflammatory cells foci (Figure 1C). In addition, significantly increased numbers of CD68$^+$ macrophages were found in livers of HFD-fed WT mice compared with diet-matched LGALS3$^{-/-}$ animals (Figure 1F). Picrosirius red (Figure 1D) and Masson trichrome (Figure 1E) staining of liver sections demonstrated HFD-induced liver fibrosis in both genotypes, but a significantly reduced amount of deposited collagen was found in LGALS3$^{-/-}$ mice. Activated α-SMA$^+$ myofibroblasts were more numerous in the livers of HFD-fed WT mice than in LGALS3$^{-/-}$ animals (Figure 1G). Moreover, significantly increased levels of hepatic procollagen type I (Figure 1E) and α-SMA (Figure 1G) mRNA expression were found in HFD-fed WT compared with diet-matched LGALS3$^{-/-}$ mice.

Enhanced Steatosis in LGALS3$^{-/-}$ Mice Is Accompanied with Alteration of Expression of Genes Related to Lipid Metabolism in Liver

We also analyzed the expression of genes related to lipid metabolism. Upon HFD, gene expression for lipogenic *LXR-β* and *SREBP-1c* increased significantly in WT mice, but not in LGALS3$^{-/-}$ mice. Transcripts for *DAG1*, *DAG2*, *CPT1*, *LXR-α*, *PPAR-γ* and *Abca-1* increased significantly in both genotypes on HFD, with significantly higher increments for *PPAR-γ* and *Abca-1* in LGALS3$^{-/-}$ mice and LXR-α in WT mice. *Cd36* and *FAS* mRNA expression was increased significantly in LGALS3$^{-/-}$ mice fed HFD compared with diet-matched WT animals (Table 2).

Decreased Number of Mature Dendritic Cells and Proinflammatory Macrophages in Livers in Gal-3-Deficient Mice on HFD

Biomarkers of liver injury (AST and ALT) increased in HFD-fed WT animals compared with diet-matched LGALS3$^{-/-}$ mice (Table 1). We then analyzed hepatic immune cell subsets. Representative flow cytometric plots and gating region used to analyze liver mononuclear cells (MNC) are shown in Supplementary Figure 1B. Upon HFD, CD11c$^+$ DCs increased in the livers of mice of both genotypes, with significantly higher numbers in WT than LGALS3$^{-/-}$ mice ($p = 0.016$). Similarly, hepatic *CD11c* mRNA levels were higher in HFD-fed WT mice as opposed to HFD-fed LGALS3$^{-/-}$ mice ($p = 0.009$; Figure 2A). Further, percentage of myeloid DCs (mDCs) (CD11c$^+$CD11b$^+$CD8a$^-$) were higher ($p = 0.001$) and lymphoid DCs (CD11c$^+$CD11b$^-$CD8a$^+$) were lower ($p = 0.008$) in WT compared with LGALS3$^{-/-}$ mice, both on HFD (Figure 2B) and higher proportions of mature myeloid DCs expressing MHCII, CD80, CD86

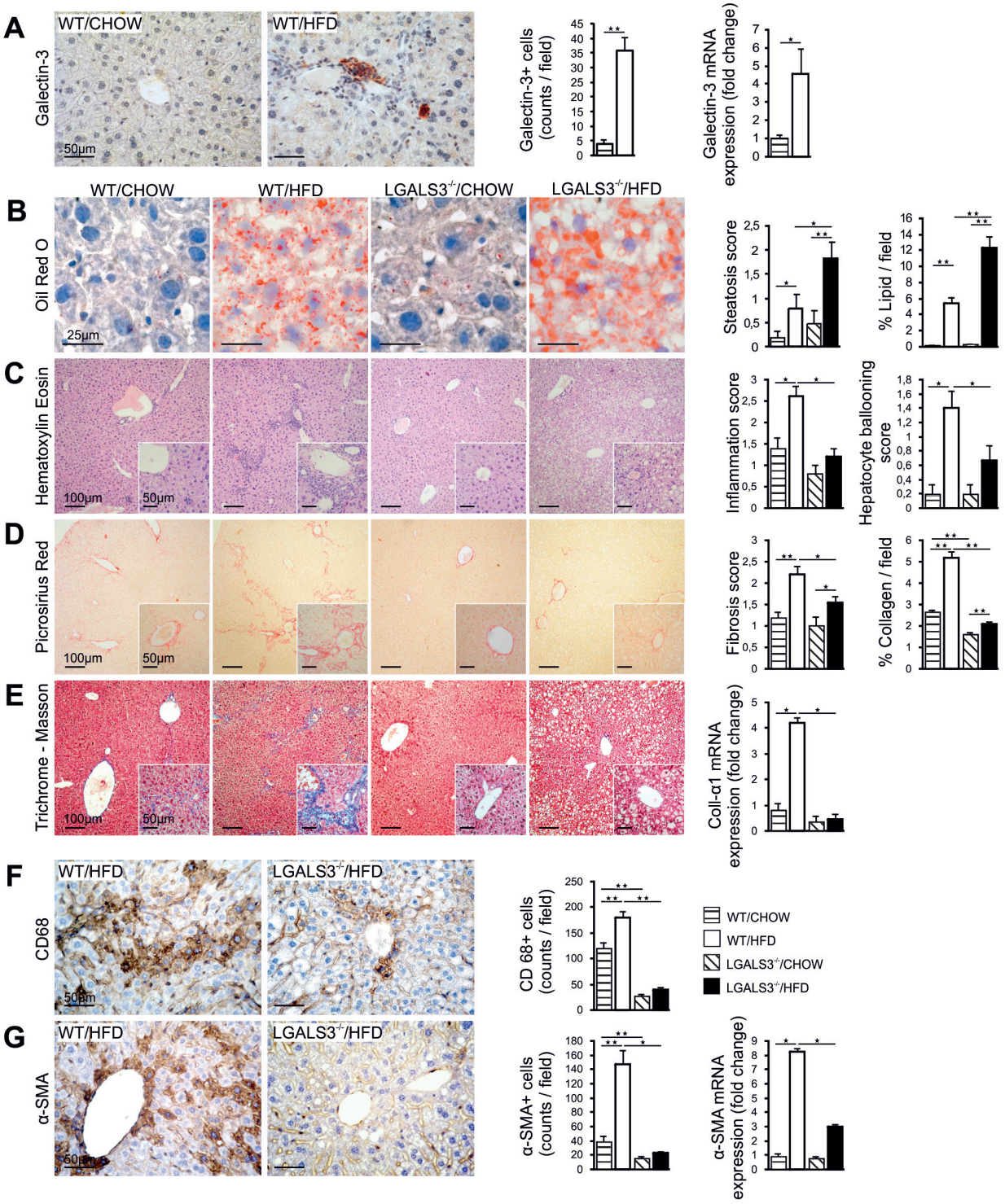

Figure 1. Increased liver steatosis but decreased inflammation and fibrosis in LGALS3$^{-/-}$ mice compared with WT mice on HFD. Representative histochemical and immunohistochemical staining of liver sections from WT and LGALS3$^{-/-}$ mice on standard diet or HFD for 24 wks. (A) Gal-3^{+} cells (40×) and mRNA expression. (B) Oil red O staining (100×). Grading of liver steatosis. (C) H&E staining (40×). Grading of liver hepatocellular injury (hepatocyte ballooning) and inflammation. (D) Picrosirius red staining (10×). Grading of liver fibrosis. (E) Masson trichrome staining (10×). Hepatic mRNA expression for procollagen1A. (F) CD68^{+} cells (40×). (G) α-SMA^{+} cells (40×) and mRNA expression. The results are shown as the means ± SEM (n = 5-6 mice/group/experiment). *P < 0.05. The results are representative of two experiments.

Table 2. Hepatic mRNA expression levels of genes involved in lipid metabolism.[a]

	WT CHOW	WT HFD	LGALS3$^{-/-}$ CHOW	LGALS3$^{-/-}$ HFD
ChREBP	1.08 ± 0.02	1.3 ± 0.23	1.27 ± 0.19	1.39 ± 0.19
LXR-α	1.02 ± 0.48	4.93 ± 0.95[b]	1.31 ± 0.66	1.65 ± 0.62[#]
LXR-β	0.93 ± 0.40	1.79 ± 0.3[b]	1.08 ± 0.27	1.42 ± 0.18
SREBP-1c	1.02 ± 0.23	1.76 ± 0.15[b]	0.89 ± 0.08	1.78 ± 0.23
PPAR-γ	1.03 ± 0.61	2.52 ± 0.53[b]	1.60 ± 0.50	5.57 ± 0.25[b,c]
Abca-1	0.32 ± 0.10	1.87 ± 0.57[b]	0.71 ± 0.30	4.87 ± 0.77[b]
Cd36	0.70 ± 0.43	1.20 ± 0.72	0.98 ± 0.56	4.70 ± 0.49[b,c]
FAS	0.66 ± 0.13	0.83 ± 0.23	0.42 ± 0.09	2.21 ± 0.31[b,c]
DAGT1	0.38 ± 0.12	1.64 ± 0.61[b]	0.33 ± 0.07	1.05 ± 0.23[b]
DAGT2	0.52 ± 0.22	3.15 ± 0.61[b]	0.51 ± 0.11	2.50 ± 0.26[b]
CPT1	0.51 ± 0.23	2.66 ± 0.87[b]	0.77 ± 0.27	2.67 ± 0.91[b]

[a]Relative mRNA expression in liver was analyzed by qRT-PCR after 24 wks of HFD or standard diet feeding. The results are shown as the means ± SEM (n = 5-6 mice/group/experiment). The results are representative of two repeated experiments.
[b]$P < 0.05$ versus CHOW-fed mice.
[c]$P < 0.05$ versus WT mice.

and CCR7 were found in the livers of WT mice (Figure 2C).

Additionally, mDCs expressing costimulatory molecule CD86 were more numerous in the bone marrow and peripheral blood of WT mice after 12 wks on HFD compared with diet-matched LGALS3$^{-/-}$ mice (Supplementary Figure 2A). Proinflammatory CD11b^{+}Ly6C^{hi}LyG^{-} monocytes ($p = 0.026$; Figure 3A), triple positive (F4/80^{+}CD11b^{+}CD11c^{+}) macrophages ($p = 0.009$; Figure 3B) and F4/80^{+}CD11c^{+}CD206^{-} M1-macrophages ($p = 0.042$; Figure 3C) were present in greater proportions, whereas F4/80^{+}CD11c^{-}CD206^{+} M2-macrophages ($p = 0.042$; Figure 3C) were lower in livers of WT compared with LGALS3$^{-/-}$ mice, both on HFD. Furthermore, proinflammatory monocytes (CD11b^{+}Ly6C^{hi}LyG^{-}) were higher in the bone marrow and peripheral blood of WT mice compared with LGALS3$^{-/-}$ animals after 12 wks of HFD feeding (Supplementary Figure 2B). Higher proportions of IL-1β-expressing F4/80^{+} macrophages were found in the livers of HFD-fed WT mice ($p = 0.008$; Figure 3B) compared with diet-matched LGALS3$^{-/-}$ mice. In addition, hepatic *F4/80*, *CCL2 NLRP3* inflammasome, *procaspase-1* and *IL-1β* mRNA expression was significantly higher in HFD-fed WT than in HFD-fed LGALS3$^{-/-}$ mice (Figure 3C). There were no differences in hepatic *TNF-α* and *IL-6* mRNA expression between WT and LGALS3$^{-/-}$ mice in response to high-fat feeding (Figure 3C).

Decreased Expression of TLR4, Proinflammatory Cytokines and Genes Related to Oxidative Stress in Livers of Gal-3-Deficient Mice on HFD

There is increasing evidence that under HFD conditions gut inflammation may enhance the interactions between intestinal bacterial products and hepatic toll-like receptors (TLR), thus promoting oxidative stress, hepatic inflammation and fibrosis. Histological examinations of colon demonstrated that there was no difference in gut inflammation in WT compared with LGALS3$^{-/-}$ mice fed HFD for 12 wks (Supplementary Figure 3A). Systemic endotoxin levels were higher in Gal-3-deficient mice compared with WT mice, both fed HFD for 12 wks (Supplementary Figure 3B). Additionally, as lipopolysaccharide (LPS) activates the TLR4 signaling pathway by binding its coreceptor CD14, we examined hepatic mRNA expression of CD14 and TLR4. Hepatic TLR4 and CD14 mRNA expression was significantly higher in HFD-fed WT mice than in HFD-fed LGALS3$^{-/-}$ mice (Supplementary Figure 3C). Levels of proinflammatory IL-1β, TNF-α and IL-17 were increased significantly in livers of HFD-fed WT mice compared with diet-matched LGALS3$^{-/-}$ mice (Supplementary Figure 4A), while the levels of IL-23, IFN-γ and IL-10 were similar (data not shown). Serum levels of IL-1β, TNF-α and IL-6 were higher in WT animals compared with LGALS3$^{-/-}$ mice, both on HFD (Supplementary Figure 4B). It is well established that activated macrophages produce reactive oxygen species (ROS) via NADPH-oxidase cascade. For that reason, we examined hepatic expression of NADPH-oxidase enzymes in WT and LGALS3$^{-/-}$ mice fed HFD for 12 wks. WT mice had significantly higher hepatic *Nox2*, *p22^{phox}*, *p47^{phox}* and *p65^{phox}* mRNA expression compared with LGALS3$^{-/-}$ mice in response to high-fat feeding for 24 wks (Figure 3E).

Gal-3 Ablation Decreases Liver Profibrotic Cytokines in Mice on HFD

In view of the fact that IL-33 is an alarmin which may be released during liver injury and has profibrogenic effects, we examined IL-33 expression in the livers of WT and LGALS3$^{-/-}$ mice on HFD for 24 wks. HFD significantly increased the numbers of IL-33-expressing hepatocytes in WT mice compared with diet-matched LGALS3$^{-/-}$ animals ($p = 0.001$; Figure 4A). Additionally, hepatic IL-33, ST2 and IL-13 mRNA expression levels were significantly elevated in WT mice compared with LGALS3$^{-/-}$ mice, both on HFD, with no differences in hepatic TGF-β mRNA expression (Figure 4B). In comparison to HFD-fed LGALS3$^{-/-}$ mice, more numerous IL-13-expressing CD11b^{+} myeloid cells were found in livers of WT mice ($p = 0.014$; Figure 4C). IL-33 and IL-13 levels were significantly higher in livers of HFD-fed WT mice compared with diet-matched LGALS3$^{-/-}$ mice (Supplementary Figure 4A). TGF-β concentrations in liver and sera were similar in both genotypes on HFD (Supplementary Figure 4). IL-13 levels in sera were higher in WT animals compared with LGALS3$^{-/-}$ mice, both on HFD, while there was no

difference in serum IL-33 levels (Supplementary Figure 4B).

Macrophages Stimulated *In Vitro* Upregulate ST2 and Produce IL-13 in Response to IL-33 Stimulation in WT but Not in LGALS3$^{-/-}$ Mice

To determine whether there are functional differences between macrophages derived from WT and LGALS3$^{-/-}$ mice, we stimulated peritoneal WT and LGALS3$^{-/-}$ macrophages with IL-33 *in vitro*. FACS analysis showed that stimulation with IL-33 significantly increased the CD11b^{+} cell population that express ST2 and IL-13 in WT mice, but this effect of IL-33 was absent in LGALS3$^{-/-}$ macrophages (Figure 4D). ELISA results validated IL-13 protein secretion from the cell culture supernatants of IL-33-stimulated macrophages. The levels of IL-13 in the cell culture supernatants of IL-33-stimulated WT macrophages were significantly higher in comparison with LGALS3$^{-/-}$ macrophages (Figure 4E).

Gal-3 Deletion Attenuates IL-33-Induced Liver Fibrosis in Mice on HFD

To determine if the differential effects of IL-33 stimulated WT and LGALS3$^{-/-}$ macrophages to produce IL-13 could be replicated *in vivo*, we injected mice with IL-33 five times every other day and collected liver for histopathological and flow cytometric analyses. We examined the effect of IL-33 administration on hepatic mononuclear cell infiltration and fibrosis in WT and LGALS3$^{-/-}$ mice both fed HFD for 12 wks. Exogenous IL-33 enhanced the number of inflammatory cells foci in the liver in both genotypes, but to a significantly lower extent in Gal-3-deficient mice ($p = 0.017$, Figure 5A). Similarly, administration of IL-33 enhanced collagen deposition in livers in both genotypes, but significantly reduced amounts of deposited collagen were found in LGALS3$^{-/-}$ mice ($p = 0.001$, Figure 5B). In addition, in mice given IL-33, a significantly elevated number of hepatic CD11b^{+} myeloid cells expressing ST2 ($p = 0.011$) and IL-13 ($p = 0.011$) were found in WT

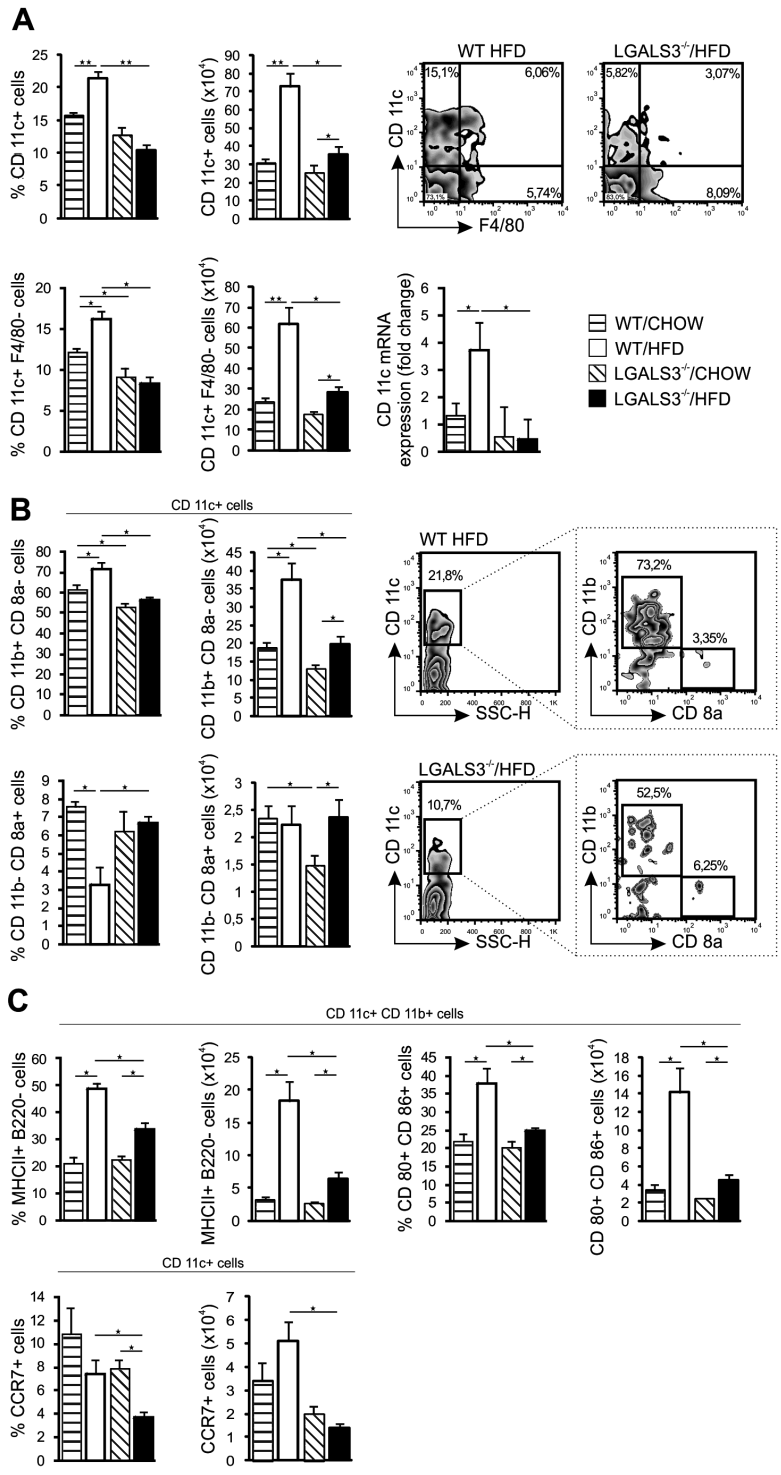

Figure 2. Decreased number of DCs in livers of LGALS3$^{-/-}$ mice on HFD. Flow cytometric analysis of liver MNCs cells from WT and LGALS3$^{-/-}$ mice after 24 wks of HFD or standard diet. (A) CD11c^{+} and CD11c^{+}F4/80^{-} DCs with representative FACS plots and CD11c mRNA expression in liver. (B) Myeloid CD11c^{+}DCs (CD11b^{+}CD8a^{-}) and lymphoid DCs (CD11b^{-}CD8a^{+}) with representative FACS plots. (C) Expression of MHC class II, CD80, CD86 and CCR7 on DCs. The results are shown as the means ± SEM (n = 5-6 mice/group/experiment). *$P < 0.05$. The results are representative of two experiments.

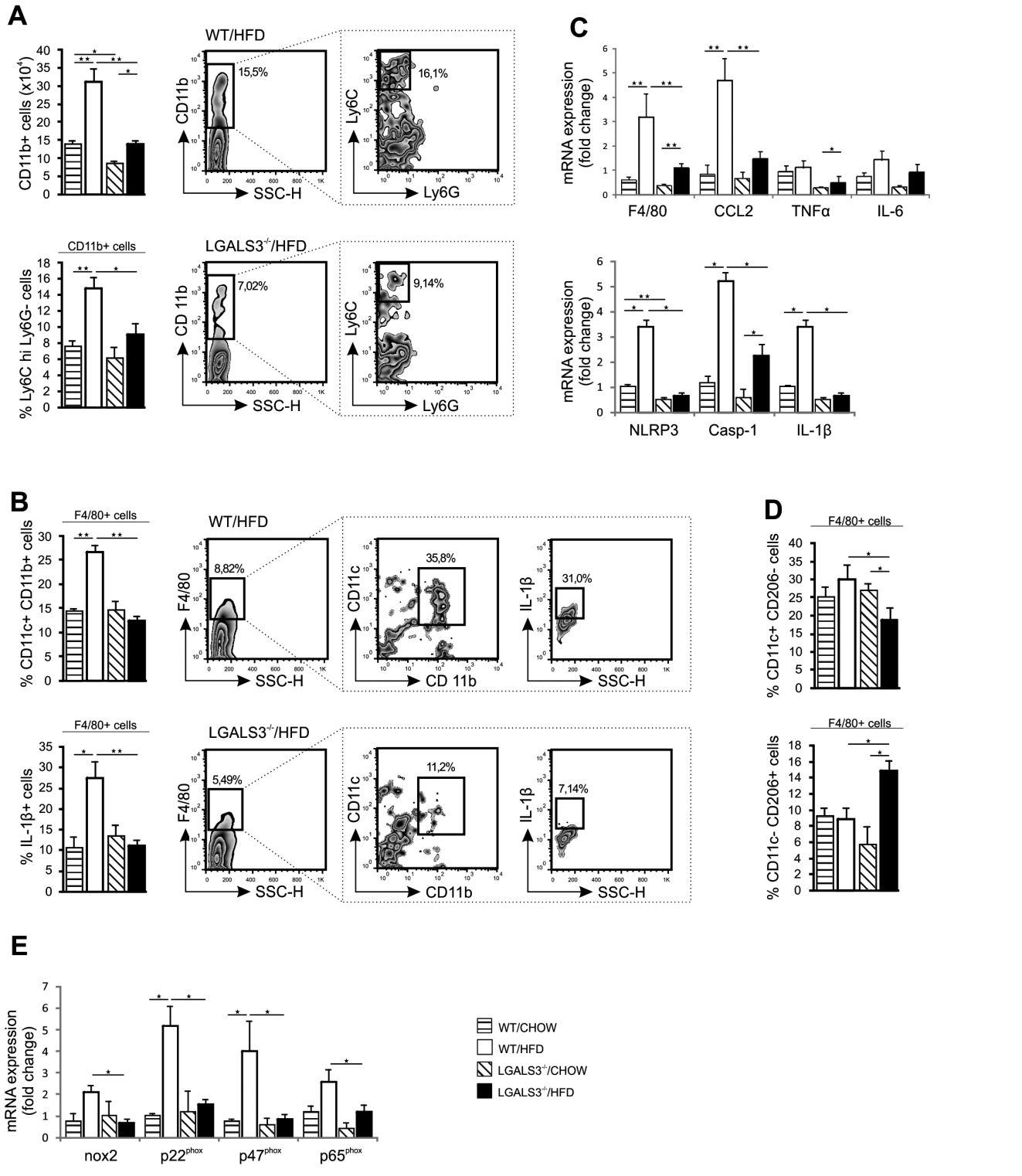

Figure 3. Galectin-3 deficiency attenuated HFD-induced recruitment of proinflammatory monocytes/macrophages in liver. Flow cytometric analysis of liver MNCs. (A) $CD11b^{+}Ly6C^{hi}Ly6G^{-}$ cells with representative FACS plots. (B) Proinflammatory macrophages with representative FACS plots. Hepatic mRNA expression for *F4/80, CCL2, TNF-α, IL-6, NLRP3, caspase-1* and *IL-1β*. (D) M1 ($F4/80^{+}CD11c^{+}CD206^{-}$) and M2 ($F4/80^{+}CD11c^{-}CD206^{+}$) macrophages. (E) Hepatic mRNA expression for *Nox2, $p22^{phox}$, $p47^{phox}$* and *$p65^{phox}$*. The results are shown as the means ± SEM (n = 5-6 mice/group/experiment). *$P < 0.05$. The results are representative of two experiments.

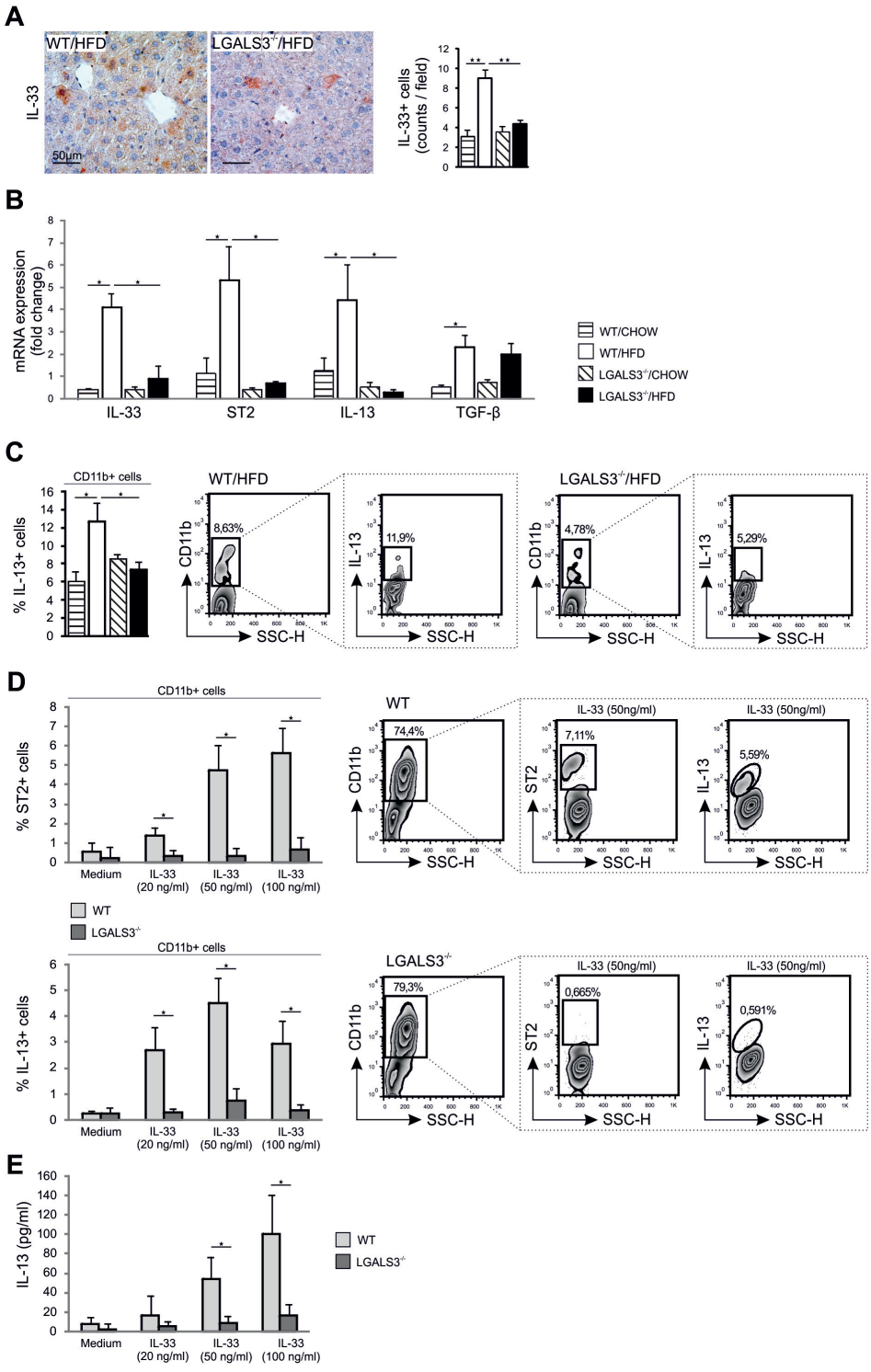

Figure 4. IL-33 expression in liver in mice on HFD. Effects of IL-33-stimulated macrophages *in vitro*. Representative immunohistochemical staining of liver sections and flow cytometric analysis of liver myeloid cells and IL-33 stimulated peritoneal macrophages. (A) IL-33$^+$ cells (40×). (B) Hepatic mRNA expression of IL-33, ST2, IL-13 and TGF-β. (C) IL-13 expressing CD11b$^+$ myeloid cells in livers of HFD or standard diet fed WT and LGALS3$^{-/-}$ mice for 24 wks. (D) Dose-dependent increase in the percentage of CD11b$^+$ST2$^+$ and CD11b$^+$IL-13$^+$ macrophages in response to *in vitro* stimulation with IL-33 (20, 50 and 100 ng/mL). (E) IL-13 levels in supernatants. The results are shown as the means ± SEM (n = 5-6 mice/group/experiment). *$P < 0.05$, **$P < 0.01$. The results are representative of two experiments.

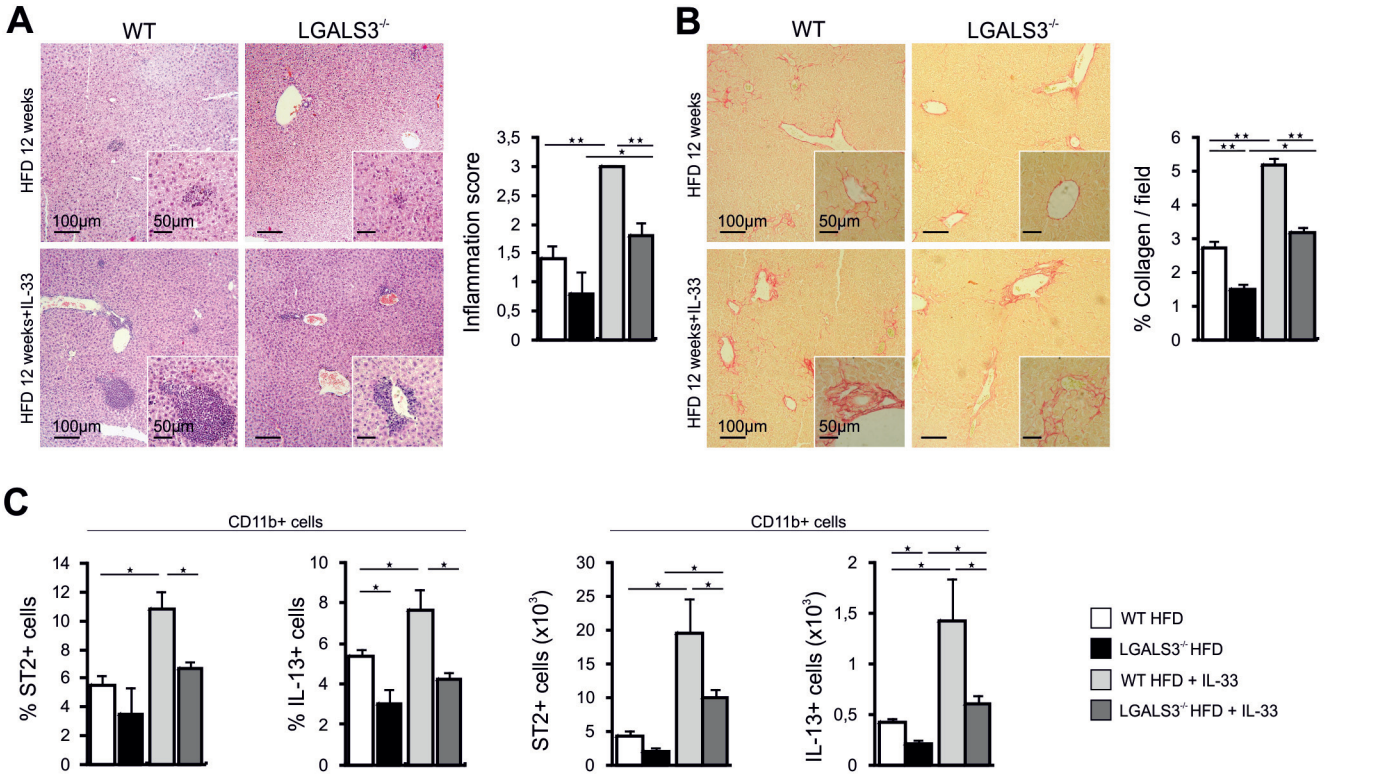

Figure 5. Galectin-3 deficiency attenuates IL-33-induced liver fibrosis in mice on HFD. The effects of *in vivo* administered IL-33 in mice fed HFD for 12 wks. (A) H&E staining (40×). Grading of liver inflammation. (B) Picrosirius red staining (10×). Grading of liver fibrosis. (C) $CD11b^+ST2^+$ and $CD11b^+IL\text{-}13^+$ cells in liver. The results are shown as the means ± SEM (n = 5-6 mice/group/experiment). $^*P < 0.05$, $^{**}P < 0.01$.

mice in comparison to $LGALS3^{-/-}$ mice (Figure 5C).

DISCUSSION

In this study, we present evidence that ablation of Gal-3 in mice fed an obesogenic high-fat diet resulted in increased obesity and visceral adipose mass, diabetes and marked liver steatosis, but attenuated liver inflammation and fibrosis (Figure 1). Incompletely defined complex immune/inflammatory pathways, which involve interaction among the adipose tissue, liver and gut, mediate the progression of steatosis to fibrotic NASH (36,37). During obesity, inflammatory response is initiated in adipose tissue and liver through various pattern recognition receptors (PRRs) in the innate immune cells, including Toll-like receptors and nucleotide-binding and oligomerization domain (NOD)-like receptors that recognize metabolic and pathogen danger molecules (38). In obesity, enhanced release of fatty acids and endotoxin through TLR4 activation in adipocytes and adipose tissue $CD11c^+$ macrophages promote the production of IL-1β, TNF-α and IL-6 which, by promoting immune cell recruitment in metabolic tissues mediate insulin resistance, contribute to steatosis and eventually NASH (37). As previously reported and shown in this study, HFD-fed Gal-3-deficient mice developed increased visceral fat mass which contained more numerous $CD11c^+$ DCs and $F4/80^+CD11b^+CD11c^+$ macrophages and increased activation of NLRP3 inflammasome and NF-κB (11), thus Gal-3 controls excessive downstream inflammation in VAT (10,11). Moreover, $LGALS3^{-/-}$ mice exhibited hyperglycemia, already noticeable in young Gal-3-deficient mice on chow and more pronounced with older mice on HFD as shown in this and previous studies and chronic hyperglycemia was confirmed by increased levels of Hb A_{1c}, hyperinsulinemia and insulin resistance (10,11).

The effects of Gal-3 ablation in HFD-fed mice on liver pathology in this study appear to be mediated by both metabolic and immunoregulatory roles of this lectin in liver. Enhanced steatosis in Gal-3-deficient mice was associated with higher hepatic expression of prosteatotic *PPAR-γ*, *Cd36*, *Abca-1* and *FAS* (Table 2). *PPAR-γ* promotes HFD-induced hepatic steatosis by induction of *Cd36* that uptakes modified lipoproteins and circulating FFA (39). Marked upregulation of *PPAR-γ* and *Cd36* in the absence of Gal-3 suggests that Gal-3 regulates primarily uptake of FFA by hepatocytes rather than *de novo* fatty acid synthesis.

Increased HFD-induced hepatic steatosis in Gal-3 deficiency was accompanied with attenuated liver injury and inflammation (Figure 1C). This was associated with downregulated *CCL2* gene, less numerous hepatic mature mDCs (Figure 2), $CD11b^+Ly6C^+$ monocytes/macrophages and $F4/80^+CD11b^+CD11c^+$ macrophages (Figure 3), the cell types that promote the development of NASH (37,40,41). Moreover, CCL2 has a crucial role in the recruitment of myeloid cells in obesity-associated liver inflammation and fibrosis (18,42). Of note, HFD-fed Gal-3-deficient mice had less numerous mature DCs and proinflammatory $CD11b^+Ly6C^{high}CCR2^+$ monocytes in the peripheral blood and bone marrow (Supplementary Figure 2). Furthermore, lower expression of hepatic *NLRP3* inflammasome, *procaspase-1* and *IL-1β* in HFD-fed $LGALS3^{-/-}$ mice (Figures 3B, C) could be the underlying mechanisms of the attenuated fibroinflammatory response in the absence of Gal-3 (43–45). In addition, HFD led to an increase of hepatic proinflammatory M1 macrophages and a decrease of antiinflammatory M2 macrophages in WT, but not in $LGALS3^{-/-}$ mice (Figure 3D). Of note, the number of M2 macrophages in livers did not differ between the genotypes on HFD (data not shown). Most recent data demonstrate that Th1/M1 type inflammatory response also triggered a Th2/M2 type response that involved hepatocyte-derived IL-33 in a model of bacterial liver infection and that these types of immune response are not mutually exclusive, but act interdependently (46). We did not find differences in gut inflammation in WT compared with $LGALS3^{-/-}$ mice fed HFD for 12 wks (Supplementary Figure 3A). Recent study shows the protective role for Gal-3 in intestine as glycans associated with mucin (MUC2) imprinted DCs with antiinflammatory properties by assembling a galectin-3-Dectin-1-FcγRIIB receptor complex (47). We show that Gal-3-deficient mice had higher serum levels of endotoxin than WT mice, both on HFD (Supplementary Figure 3B). The proinflammatory effects of endotoxin might be attenuated in liver in $LGALS3^{-/-}$ mice, as lower expression of hepatic *TLR4*, *CD14* and NADPH-oxidase enzymes were found in Gal-3 absence.

Gal-3 deletion attenuated HFD-induced liver fibrosis as evaluated by lower fibrosis score, lower expression of hepatic procollagen and α-SMA and lower number of α-SMA + myofibroblasts than in WT mice (Figure 1). We demonstrate a higher number of Gal-3 positive macrophage-like cells and higher hepatic Gal-3 mRNA expression in WT mice upon HFD (Figure 1A) which also had increased numbers of activated hepatic CD68 + macrophages (Figure 1F). In mice on HFD, the lack of Gal-3 resulted in lower levels of IL-17 in liver. Recent evidence shows that activation of the IL-17 axis in obesity-driven NAFLD has an important role in the progression of liver steatosis to NASH (30). The data of attenuated liver inflammation in $LGALS3^{-/-}$ mice fed obesogenic HFD in this study are in agreement with the data in the study of the atherogenic diet model of NASH (15).

Importantly, in HFD-fed $LGALS3^{-/-}$ mice, hepatic IL-33, ST2 (IL-33 receptor) and IL-13 mRNA expression and IL-33 and IL-13 levels were lower in liver homogenates compared with WT mice (Supplementary Figures 4A, B). At variance with the reported data obtained with the atherogenic diet-induced NASH (15), the levels and hepatic *TGF-β* mRNA expression were comparable between the two genotypes in our study (Figure 4B). It has been proposed that the IL-33/IL-13 axis promotes liver fibrosis (25). A number of different cell types have been identified as candidates for IL-13 production upon IL-33 stimulation, including T cells and macrophages (24,48,49). In contrast to WT mice, livers of HFD-fed $LGALS3^{-/-}$ mice contained lower proportions of IL-13 expressing $CD11b^+$ myeloid cells (Figure 4C), but not $CD3^+$ T cells and $Lin^-Sca\text{-}1^+$ innate lymphoid cells (data not shown). The role of IL-33 in HFD-induced liver fibrosis appears to be mediated via an increased IL-13 production. We present evidence that *in vivo* administration of IL-33 led to increased liver fibrosis in both genotypes on HFD, but to a significantly lesser extent in Gal-3-deficient mice, which was accompanied with less numerous $CD11b^+$ cells expressing ST2 and IL-13 (Figures 4D, E), while the percentages and numbers of $Lin^-Sca\text{-}1^+$ innate lymphoid cells expressing IL-13 did not differ between genotypes (data not shown). Moreover, we show that *in vitro* stimulation of WT peritoneal macrophages with IL-33 increased percentages of $ST2^+$ and $IL\text{-}13^+$ $CD11b^+$ cells, whereas this effect was absent in $LGALS3^{-/-}$ macrophages (Figure 5C). Thus, this is the first demonstration that Gal-3 regulates IL-33/ST2-dependent ST2 expression and IL-13 production in macrophages, which may represent the additional mechanism involved in the profibrogenic effects of Gal-3.

CONCLUSION

In summing up, we provide evidence that Gal-3 attenuates steatosis but promotes liver injury, inflammation and fibrosis in an obesogenic mouse model of NASH; thus Gal-3 is involved in the progression of NASH (Figure 6). Further, we show for the first time that newly described profibrogenic IL-33/ST2/IL-13 pathway is Gal-3 dependent.

ACKNOWLEDGMENTS

We thank Ivan Jovanovic, Gordana Radosavljevic and Ivana Stojanovic for collegial help and Aleksandar Ilic, Katerina Martinova, Sandra Nikolic (Center for Molecular Medicine, Faculty of Medical Sciences, University of Kragujevac) and Zoran Mitrovic (Institute of Pathology, Faculty of Medical Sciences, University of Kragujevac) for technical assistance. This work was

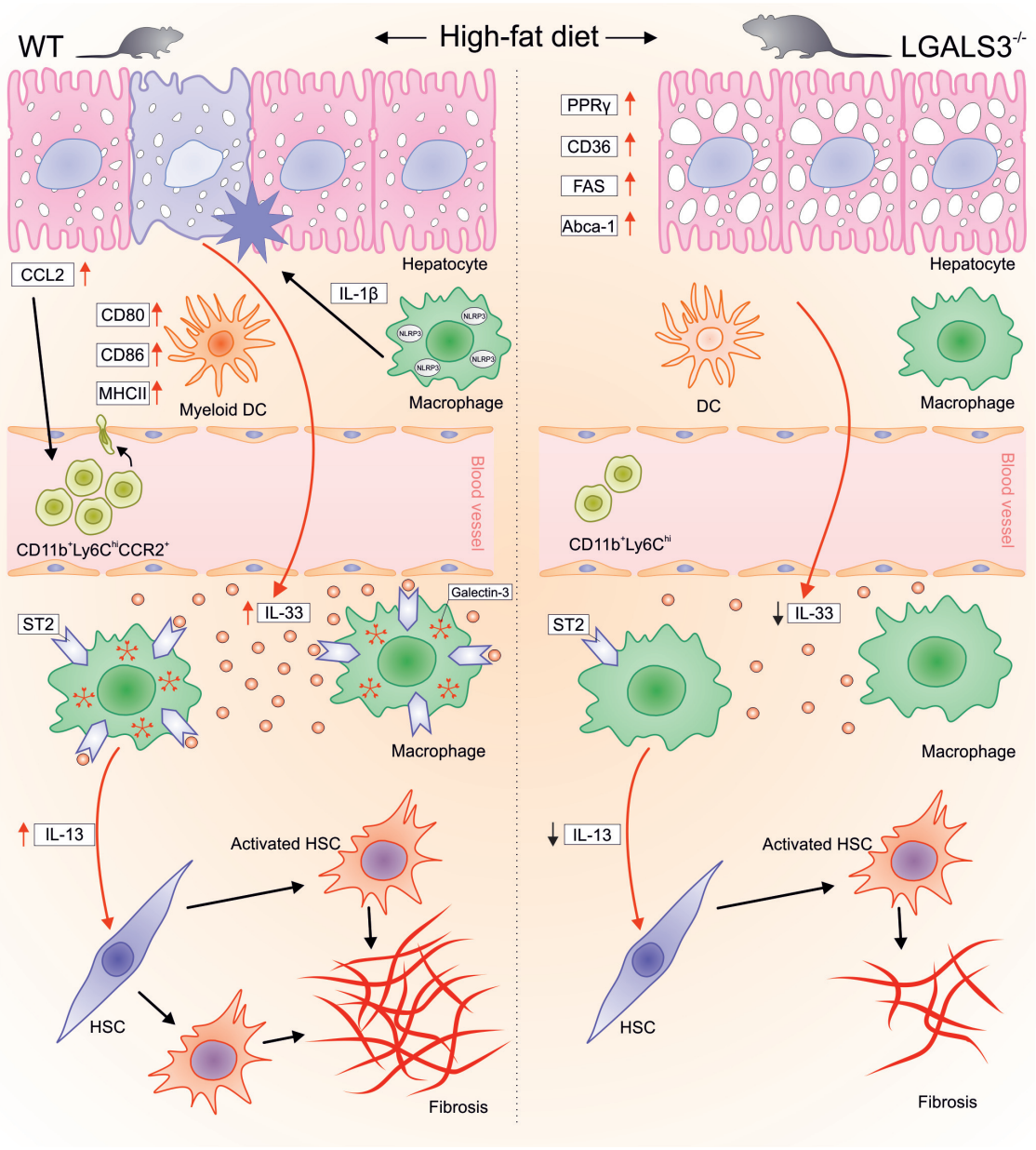

Figure 6. Gal-3 differentially regulates staetosis, liver inflammation and fibrosis in a obesogenic mouse model of fibrotic NASH. In Gal-3-deficient mice, obesogenic HFD increased adiposity and steatosis, but liver inflammation and fibrosis were attenuated compared with WT mice. Reduced hepatic fibroinflammatory response in LGALS3$^{-/-}$ mice was associated with less numerous proinflammatory mature mDCs, CD11b^{+}Ly6C^{hi} and F4/80^{+}CD11b^{+}CD11c^{+} macrophages, lower expression of CCL2, NLRP3 inflammasome, IL-1β, IL-33, ST2 and IL-13 in liver. Events proposed in the scheme are supported by *in vitro* data showing that, in contrast to WT cells, LGALS3$^{-/-}$ peritoneal macrophages failed to upregulate ST2 expression and IL-13 production in response to IL-33 stimulation and that *in vivo* administered IL-33 enhanced liver fibrosis in both genotypes on HFD, but to a significantly lower extent in the absence of Gal-3 (see Results).

supported by grants from the Serbian Ministry of Science and Technological Development (175071 and 175069) (Belgrade, Serbia), Swiss Science Foundation (SCOPES, IZ73Z0_152407) and junior faculty grants (JP 02-14, JP 03-14) Faculty of Medical Sciences, Kragujevac, Serbia.

DISCLOSURE

The authors declare they have no competing interests as defined by *Molecular Medicine*, or other interests that

might be perceived to influence the results and discussion reported in this paper.

REFERENCES

1. Lumeng CN, Saltiel AR. (2011) Inflammatory links between obesity and metabolic disease. *J. Clin. Invest*. 121:2011–7.
2. Chalasani N, *et al*. (2012) The diagnosis and management of non-alcoholic fatty liver disease: practice Guideline by the American Association for the Study of Liver Diseases, American College of Gastroenterology, and the American Gastroenterological Association. *Hepatology*. 55:2005–23.
3. Day CP, James OF. (1998) Steatohepatitis: a tale of two "hits"? *Gastroenterology*. 114:842–5.
4. Friedman, S.L. (2010) Evolving challenges in hepatic fibrosis. *Nat. Rev. Gastroenterol. Hepatol*. 7:425–36.
5. Dumic J, *et al*. (2006) Galectin-3: an open-ended story. *Biochim. Biophys. Acta*. 1760:616–35.
6. Liu FT. (2005) Regulatory roles of galectins in the immune response. *Int. Arch. Allergy. Immunol*. 136:385–400.
7. Henderson NC, *et al*. (2009) The regulation of inflammation by galectin-3. *Immunol. Rev*. 230:160–71.
8. Radosavljevic G, *et al*. (2010) The roles of Galectin-3 in autoimmunity and tumor progression. *Immunol. Res*. 52:100–10.
9. Li Y, *et al*. (2008) Galectin-3 is a negative regulator of lipopolysaccharide-mediated inflammation. *J. Immunol*. 181:2781–9.
10. Pang J, *et al*. (2013) Increased adiposity, dysregulated glucose metabolism and systemic inflammation in galectin-3 KO mice. *PLoS One*. 8:e57915.
11. Pejnovic NN, *et al*. (2013) Galectin-3 deficiency accelerates high-fat diet-induced obesity and amplifies inflammation in adipose tissue and pancreatic islets. *Diabetes*. 62:1932–44.
12. Iacobini C, *et al*. (2009) Accelerated lipid-induced atherogenesis in galectin-3 deficient mice: role of lipoxidation via receptor-mediated mechanisms. *Arterioscler. Thromb. Vasc. Biol*. 29:831–6.
13. Nomoto K, *et al*. (2006) Disrupted galectin-3 causes non-alcoholic fatty liver disease in male mice. *J. Pathol*. 210:469–77.
14. Nomoto K, *et al*. (2008) Nonalcoholic steatohepatitis and hepatocellular carcinoma in galectin-3 knockout mice. *Hepatol. Res*. 38:1241–51.
15. Iacobini C, *et al*. (2011) Galectin-3 ablation protects mice from diet-induced NASH: A major scavenging role for galectin-3 in liver. *J. Hepatol*. 54:975–83.
16. Hsu DK, *et al*. (1999) Galectin 3 expression is induced in cirrhotic liver and hepatocellular carcinoma. *Int. J. Cancer*. 81:519–26.
17. Baeck C, *et al*. (2012) Pharmacological inhibition of the chemokine CCL2 (MCP-1) diminishes liver macrophage infiltration and steatohepatitis in chronic hepatic injury. *Gut*. 61:416–26.
18. Miura K, Yang L, van Rooijen N, Ohnishi H, Seki E. (2012) Hepatic recruitment of macrophages promotes nonalcoholic steatohepatitis through CCR2. *Am. J. Physiol. Gastrointest. Liver. Physiol*. 302:1310–21.
19. Tacke F, Zimmermann HW. (2014) Macrophage heterogeneity in liver injury and fibrosis. *J. Hepatol*. 60:1090–6.
20. Martinez FO, Sica A, Mantovani A, Locati M. (2008) Macrophage activation and polarization. *Front. Biosci*. 13:453–61.
21. Pellicoro A, Ramachandran P, Iredale JP, Fallowfield JA. (2014) Liver fibrosis and repair: immune regulation of wound healing in a solid organ. *Nat. Rev. Immunol*. 14:181–94.
22. Henderson NC, *et al*. (2006) Galectin-3 regulates myofibroblast activation and hepatic fibrosis. *Proc. Natl. Acad. Sci. U.S.A*. 103:5060–5.
23. Li LC, Li J, Gao J. (2014) Functions of galectin-3 and its role in fibrotic diseases. *J. Pharmacol. Exp. Ther*. 351:336–43.
24. Yang Z, *et al*. (2013) Macrophages as IL-25/IL-33-responsive cells play an important role in the induction of type 2 immunity. *PLoS One*. 8:e59441.
25. Mchedidze T, *et al*. (2013) Interleukin-33-dependent innate lymphoid cells mediate hepatic fibrosis. *Immunity*. 39:357–71.
26. Palmer G. and Gabay C. (2011) Interleukin-33 biology with potential insights into human diseases. *Nat. Rev. Rheumatol*. 7:321–9.
27. Liu Y, *et al*. (2011) IL-13 induces connective tissue growth factor in rat hepatic stellate cells via TGF-β-independent Smad signaling. *J. Immunol*. 187:2814–23.
28. Matthews DR, *et al*. (1985) Homeostasis model assessment: insulin resistance and beta-cell function from fasting plasma glucose and insulin concentrations in man. *Diabetologia*. 28:412–9.
29. Kleiner DE, *et al*. (2005) Design and validation of a histological scoring system for nonalcoholic fatty liver disease. *Hepatology*. 41:1313–21.
30. Harley IT, *et al*. (2014) IL-17 signaling accelerates the progression of nonalcoholic fatty liver disease in mice. *Hepatology*. 59:1830–9.
31. Deutch MJ, Schriever SC, Roscher AA, Ensenauer R. (2014) Digital image analysis approach for lipid droplet size quantitation of Oil Red O-stained cultured cells. *Anal. Biochem*. 445:87–9.
32. Hadi AM, *et al*. (2010) Rapid quantification of myocardial fibrosis: A new macro-based automated analysis. *Anal. Cell. Pathol. (Amst)*. 33:257–69.
33. Volarevic V, *et al*. (2012) Protective role of IL-33/ST2 axis in Con A-induced hepatitis. *J. Hepatol*. 56:26–33.
34. Trotier MD, Naaz A, Li Y, Fraker PJ. (2012) Enhancement of hematopoiesis and lymphopoiesis in diet-induced obese mice. *Proc. Natl. Acad. Sci. U.S.A*. 109:7622–9.
35. Livak KJ and Schmittgen TD. (2001) Analysis of relative gene expression data using real-time quantitative PCR and the 2(-Delta Delta C(T)) method. *Methods*. 25:402–8.
36. Stanton MC, *et al*. (2011) Inflammatory signals shift from adipose to liver during high fat feeding and influence the development of steatohepatitis in mice. *J. Inflamm. (Lond.)*. 8:8.
37. Nguyen MT, *et al*. (2007) A subpopulation of macrophages infiltrates hypertrophic adipose tissue and is activated by free fatty acids via Toll-like receptors 2 and 4 and JNK-dependent pathways. *J. Biol. Chem*. 282:35279–92.
38. Ganz M, Szabo G. (2013) Immune and inflammatory pathways in NASH. *Hepatol. Int*. 7:771–81.
39. Jie Zhou, *et al*. (2008) hepatic fatty acid transporter Cd36 is a common target of LXR, PXR, and PPAR-γ in promoting steatosis. *Gastroenterology*. 134:556–67.
40. Patsouris D, *et al*. (2008) Ablation of CD11c-positive cells normalizes insulin sensitivity in obese insulin resistant animals. *Cell. Metabolism*. 8:301–9.
41. Stefanovic-Racic M, *et al*. (2012) Dendritic cells promote macrophage infiltration and comprise a substantial proportion of obesity-associated increases in CD11c+ cells in adipose tissue and liver. *Diabetes*. 61:2330–9.
42. Obstfeld AE, *et al*. (2010) C-c chemokine receptor 2 (CCR2) regulates the hepatic recruitment of myeloid cells that promote obesity-induced hepatic steatosis. *Diabetes*. 59:916–25.
43. Csak T, *et al*. (2011) Fatty acid and endotoxin activate inflammasomes in mouse hepatocytes that release danger signals to stimulate immune cells. *Hepatology*. 54:133–44.
44. Miura K, *et al*. (2010) Toll-like receptor 9 promotes steatohepatitis by induction of interleukin-1beta in mice. *Gastroenterology*. 139:323–34.
45. Dixon LJ, Berk M, Thapaliya S, Papouchado BG, Feldstein AE. (2012) Caspase-1-mediated regulation of fibrogenesis in diet-induced steatohepatitis. *Lab. Invest*. 92:713–23.
46. Bléroit C, *et al*. (2015) Liver-resident macrophage necroptosis orchestrates type 1 microbicidal inflammation and type-2-mediated tissue repair during bacterial infection. *Immunity*. 42:145–58.
47. Shan M, *et al*. (2013) Mucus enhances gut homeostasis and oral tolerance by delivering immunoregulatory signals. *Science*. 342:447–53.
48. Li D, *et al*. (2014) IL-33 promotes ST2-dependent lung fibrosis by the induction of alternatively activated macrophages and innate lymphoid cells in mice. *J. Allergy. Clin. Immunol*. 134:1422-32.e11.
49. Milovanovic M, *et al*. (2012) IL-33/ST2 axis in inflammation and immunopathology. *Immunol. Res*. 52:89–99.

Cite this article as: Jeftic I, *et al*. (2015) Galectin-3 ablation enhances liver steatosis, but attenuates inflammation and IL-33-dependent fibrosis in obesogenic mouse model of nonalcoholic steatohepatitis. *Mol. Med*. 21:453–65.